Surface Science 604 (2010) 1425–1431

Contents lists available at ScienceDirect

Surface Science

journal homepage: www.elsevier.com/ locate/susc

Role of sub-surface oxygen in Cu(100) oxidation

Minyoung Lee, Alan J.H. McGaughey *

Department of Mechanical Engineering, Carnegie Mellon University, Pittsburgh, PA 15213, United States

ARTICLE INFO

Article history:
Received 18 March 2010
Accepted 3 May 2010
Available online 17 May 2010

Keywords:
Copper (100) oxidation
Sub-surface oxygen
Missing-row reconstruction
Oxygen-induced restructuring
Density functional theory

ABSTRACT

Density functional theory (DFT) calculations are used to investigate the role of sub-surface oxygen in Cu(100) oxidation. We find that the presence of sub-surface oxygen atoms causes the top copper layer of the missing-row reconstructed surface to rise by 1.7 Å compared to the bare surface. This prediction compares well to an earlier scanning tunneling microscopy measurement of 1.8 Å [Lampimaki et al. Journal of Chemical Physics 126 (2007) 034703]. When the missing-row reconstructed surface is exposed to an additional oxygen molecule, surface restructuring that leads to oxide-like structures is only observed when sub-surface oxygen is present. The oxide-like nature of these structures is confirmed through structural, Bader, and electron density of states analyses. These findings, combined with our previous DFT results that predicted low energy barriers for the embedment of oxygen atoms into the sub-surface [Lee and McGaughey, Surface Science 603 (2009) 3404], demonstrate the key role played by sub-surface oxygen in Cu(100) oxidation.

1. Introduction

Copper and its oxides (CuO and Cu_2O) are relevant in many scientific and engineering applications. Cu_2O, which is a direct band gap semiconductor, is a candidate material for next-generation photovoltaic cells [1,2]. During the electrochemical reaction in a solid state cell containing Cu^+ conducting electrolytes, a Cu/Cu_2O interface is formed and detrimentally affects the cell performance [3]. To prevent CO poisoning, copper, CuO, and Cu_2O powders and nanoparticles are being considered as substitutes for the platinum catalyst in fuel cells [4,5]. It is thus important to understand the atomistic structure and energetics of copper–oxide interfaces and how the associated free surfaces interact with their environments.

Based on the existing experimental and theoretical data, the oxidation of a Cu(100) surface is a four-step process that proceeds as more oxygen molecules arrive at the surface: (i) Oxygen molecules dissociate and the oxygen atoms adsorb on the face-centered cubic (fcc) hollow sites up to 0.5 monolayer (ML) coverage [$c(2\times2)$ phase] [6–17]. (ii) The $\left(2\sqrt{2}\times\sqrt{2}\right)$R45° missing-row reconstruction is formed by the release of every fourth row of copper atoms from the top copper layer [18–29]. (iii) Merged missing-row reconstructed domains are formed and Cu_2O islands nucleate [30,31]. (iv) Islands grow and merge with other islands to form a continuous oxide layer [32–36]. This behavior is different from typical metal-oxides (e.g., aluminium, iron, and barium), which grow as a uniform layer on a clean metal surface [37]. The shapes of the Cu_2O islands in steps (iii) and (iv) vary with the oxidation temperature. They are triangles at 350 °C, squares at 500 °C, high aspect-ratio nanorods at 600 °C, and pyramids above 700 °C [34]. To use (and potentially control) the varied nanostructures of the Cu_2O islands, an understanding of the atomic-level mechanisms of copper oxidation is needed.

There have been theoretical and experimental investigations of the atomic oxygen adsorption [step (i)] [6–17] and the oxygen-induced surface reconstruction [step (ii)] [18–29]. A limited number of investigations, however, have studied the transition from the missing-row reconstruction to Cu_2O island formation [step (iii)] [30,31,38–40]. Using scanning tunneling microscopy (STM), Lampimaki et al. observed that individual missing-row reconstructions merge to form an ordered domain that is 1.8 Å higher than the clean surface. They found that Cu_2O islands form on these domains [30]. They suggest that the copper atoms released during the missing-row reconstruction form an adlayer that subsequently reconstructs due to further oxygen adsorption. This process elevates the surface and creates sub-surface oxygen. As we previously reported, however, oxygen can also directly penetrate into the sub-surface region through the missing row. Lahtonen et al. found, using STM and X-ray photoelectron spectroscopy, that oxygen penetration into the sub-surface region plays a key role in the subsequent oxidation and the growth of Cu_2O islands [31]. Using density functional theory (DFT) calculations, Kangas et al. found that a missing-row reconstructed Cu(100) surface that includes on- and sub-surface oxygen atoms is more energetically favorable than a missing-row reconstructed surface including only on-surface oxygen atoms [38]. Using DFT calculations, Kangas and Laasonen later found that oxygen embeds into the sub-surface more easily when there are adsorbed oxygen atoms both on the surface and in the sub-surface [39]. They also found significant structural changes on the missing-row reconstructed Cu (100) surface when the sub-surface oxygen coverage increases from 0.25 to 1.0 ML. The unit cell $\left[p\left(\sqrt{2}\times\sqrt{2}\right)\right]$ used in that study, however, was too small for the authors to identify possible Cu_2O-like structures and the transition mechanism from the missing-row reconstructed

* Corresponding author.
E-mail address: mcgaughey@cmu.edu (A.J.H. McGaughey).

0039-6028/$ – see front matter © 2010 Elsevier B.V. All rights reserved.
doi:10.1016/j.susc.2010.05.004

surface to Cu_2O island nucleation. In a previous report, we used DFT calculations to show that oxygen embedment into the Cu(100) surface and sub-surface diffusion are possible mechanisms for driving this transition [40].

The objective of this work is to use DFT calculations to further investigate the transition from the missing-row reconstructed Cu(100) surface to Cu_2O island formation [step (iii)]. In Section 2, the computational unit cells, set-up, and procedures are presented. In Section 3.1, we investigate the relative stabilities of unreconstructed and reconstructed Cu(100) surfaces. In Section 3.2, we analyze the energetic and structural changes induced when an oxygen molecule interacts with missing-row reconstructed Cu(100) surfaces for different on- and sub-surface oxygen coverages. In Section 4, we summarize our findings.

2. Calculation methodology

Our DFT calculations are performed using the Vienna Ab-initio Simulation Package (VASP) [41–45], which uses a plane-wave basis set [43,45]. We use ultra-soft pseudo potentials, the PW91 generalized gradient approximation [46], and apply a 350 eV energy cutoff. The $p(2\times2)$ unit cell is used for the unreconstructed surface and the $p\left(2\sqrt{2}\times2\sqrt{2}\right)$ and $p\left(4\sqrt{2}\times4\sqrt{2}\right)$ unit cells are used for the missing-row reconstructed surface. All the slab structures include 5 copper layers (with the bottom layer fixed) and a vacuum gap thickness of 11 Å. There are 152 copper and 48 oxygen atoms in the $p\left(4\sqrt{2}\times4\sqrt{2}\right)$ unit cell with a sub-surface oxygen coverage of 1.0 ML, the largest that we consider. The k-point mesh is generated by the Monkhorst–Pack scheme [47]. We use an $8\times8\times1$ mesh for the $p(2\times2)$ and $p\left(2\sqrt{2}\times2\sqrt{2}\right)$ unit cells, and a $4\times4\times1$ mesh for the $p\left(4\sqrt{2}\times4\sqrt{2}\right)$ unit cell.

To induce further restructuring, we add an oxygen molecule to the missing-row structures. The initial positions are shown in Fig. 1(a) and (b). The copper atom located at the step-edges next to the missing row is labeled Cu_S. The topmost copper atoms located between the copper atoms at the step-edges are labeled Cu_C.

The on- and sub-surface oxygen sites for the unrelaxed reconstructed surface are shown in Fig. 2(a) and (b). "Hol" and "octa" refer to the fcc hollow and octahedral sites, consistent with the notation used in our previous report [40]. In the $p\left(2\sqrt{2}\times2\sqrt{2}\right)$ unit cell, there are two identical locations for each hol and octa site. The label "2hol7" represents the missing-row reconstructed surface with every hol7 site occupied. "octa23" represents a surface with one octa2 site and one octa3 site occupied. In the "2octa23" structure, every octa2 and octa3 site is occupied.

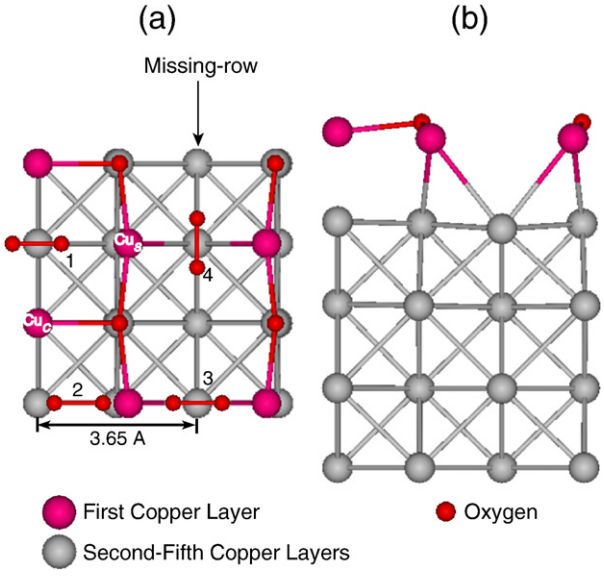

Fig. 1. Initial positions of the oxygen molecule on the missing-row reconstructed Cu (100) surface. (a) Top and (b) side view of the $p\left(2\sqrt{2}\times2\sqrt{2}\right)$ unit cell at 0.5 ML coverage: 1. fcc hollow site (FCC). 2. Between fcc and Cu_S (BFC). 3. Perpendicular to missing row (PMR). 4. Parallel to missing row (RMR). The oxygen molecules are only shown in (a).

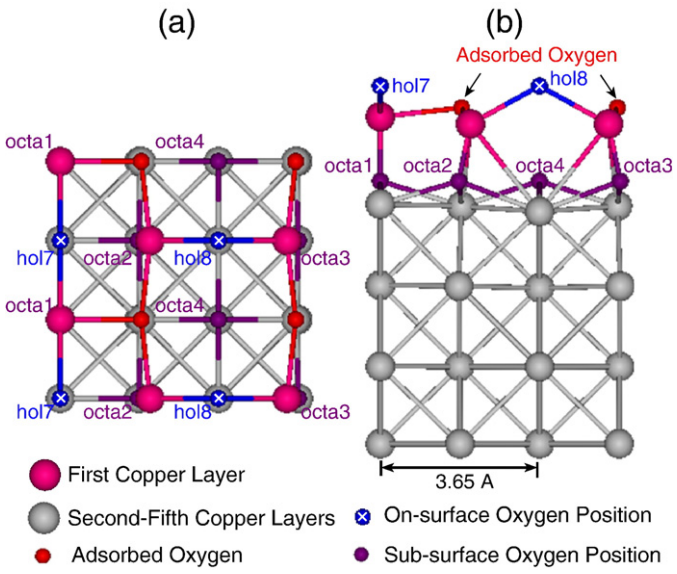

Fig. 2. (a) Top and (b) side views of the unrelaxed missing-row reconstructed Cu(100) surface with on- and sub-surface oxygen atoms in the $p\left(2\sqrt{2}\times2\sqrt{2}\right)$ unit cell.

The relative stabilities of the relaxed structures described in Sections 3.1 and 3.2 are compared using the surface-oxide energy, E_S [40,48]:

$$E_S = \frac{E_{O/Cu} - N_{Cu}\cdot E_{Cu,bulk} - N_O\cdot\frac{E_{O_2}}{2}}{A_{surf}}. \quad (1)$$

Here, $E_{O/Cu}$ is the total system energy, $E_{Cu,bulk}$ is the energy of one atom in bulk fcc copper, and E_{O_2} is the energy of an isolated oxygen molecule. N_O and N_{Cu} are the total number of oxygen and copper atoms in the system and A_{Surf} is the unit cell surface area. Because E_S is normalized by the unit cell area, it can be used to compare surfaces with different unit cell sizes. A spin-polarized DFT calculation is used to obtain E_{O_2}. Spin-averaged calculations are used for all other calculations.

We performed convergence tests for the $p\left(2\sqrt{2}\times2\sqrt{2}\right)$ missing-row reconstructed surface for the number of k-points, the energy cutoff, and the number of copper layers. The total energy difference between $8\times8\times1$ and $12\times12\times1$ k-point meshes is 0.005 eV (9.4×10^{-5} eV/Å^2). The total energy difference between 350 eV and 600 eV energy cutoffs is 0.005 eV. The surface-oxide energy difference between 5 and 8 copper layers is 7.7×10^{-4} eV/Å^2. Based on the magnitudes of these energy differences, we believe that the energies reported in Section 3 are sufficiently accurate to allow us to compare the stabilities of and structural changes in different structures.

3. Oxygen-induced surface restructuring

3.1. Relative stabilities of surfaces relaxed without an oxygen molecule

In Table 1, we report the surface-oxide energy and the height of the top copper layer measured from that of the clean Cu(100) surface for different oxygen coverages.[1] No additional oxygen molecules are

[1] Using an energy cutoff of 330 eV, we previously reported the E_S of $c(2\times2)$, mr, and $p(2\times2)$ to be 0.049, 0.039, and 0.040 eV/Å^2 [40]. Based on the energy cutoff convergence test discussed in Section 2, we believe that the results presented in Table 1 are more accurate.

Table 1
Surface-oxide energy, E_S, and height change for different on- and sub-surface oxygen coverages. The unit cell area is 26.645 Å^2 for $p(2\times2)$ and 53.290 Å^2 for $p\left(2\sqrt{2}\times2\sqrt{2}\right)$. "U" and "R" represent unreconstructed and reconstructed surfaces. Oxygen coverages are shown for on-surface (On-) and sub-surface (Sub-) separately. 2octa2, 2octa23, 2octa123, and 2octa1234 are missing-row reconstructed (mr) surfaces relaxed with sub-surface oxygen atoms [see Fig. 2(a) and (b)].

Index	U or R	On- [ML]	Sub- [ML]	Unit Cell	E_S [eV/Å^2]	Height [Å]
Clean	U	0.00	0.00	$p\left(2\sqrt{2}\times2\sqrt{2}\right)$	0.184	0.00
$c(2\times2)$	U	0.50	0.00	$p\left(2\sqrt{2}\times2\sqrt{2}\right)$	0.047	0.89
mr	R	0.50	0.00	$p\left(2\sqrt{2}\times2\sqrt{2}\right)$	0.045	0.32
$p(2\times2)$	U	0.75	0.00	$p(2\times2)$	0.047	0.44
$p(1\times1)$	U	1.00	0.00	$p(2\times2)$	0.070	0.36
2octa2	R	0.50	0.25	$p\left(2\sqrt{2}\times2\sqrt{2}\right)$	0.010	1.16
2octa23	R	0.50	0.50	$p\left(2\sqrt{2}\times2\sqrt{2}\right)$	−0.030	1.72
2octa123	R	0.50	0.75	$p\left(2\sqrt{2}\times2\sqrt{2}\right)$	−0.057	1.74
2octa1234	R	0.50	1.00	$p\left(2\sqrt{2}\times2\sqrt{2}\right)$	−0.051	1.75

present. For the unreconstructed surfaces [clean, $c(2\times2)$, $p(2\times2)$, and $p(1\times1)$], E_S decreases with increasing oxygen coverage from 0 ML to 0.50 ML then increases from 0.75 ML to 1.0 ML. This result indicates that there is an energetically stable structure between coverages of 0.5 ML and 0.75 ML. At an oxygen coverage of 0.5 ML, E_S of the missing-row reconstructed (mr) surface is smaller than that of $c(2\times2)$. The missing-row reconstruction is thus more energetically favorable than $c(2\times2)$. We note that while the E_S difference is small and sensitive to the DFT calculation parameters, this result agrees with previous experimental and modeling works [18–29], indicating that the missing-row reconstructed surface is the stable transition state from a clean copper surface to copper–oxide island nucleation.

For the reconstructed surfaces (mr, 2octa2,[2] 2octa23, 2octa123, and 2octa1234), the on-surface oxygen coverage is fixed at 0.5 ML and the sub-surface oxygen coverage is increased from 0 (mr) to 1.0 ML (2octa1234). As the sub-surface oxygen coverage increases, E_S decreases, and the minimum E_S is predicted at a total coverage of 1.25 ML (2octa123). In all cases with sub-surface oxygen, there is a notable elevation of the top copper layer and structural changes [compare Fig. 3(c) and (d) to Fig. 3(a) and (b)]. The smaller E_S values indicate that sub-surface oxygen makes the surfaces more energetically stable, as found by others [38,39].

We previously argued for the presence of sub-surface oxygen by showing that the energy barriers for oxygen embedment are comparable to those for on-surface diffusion [40]. Further proof for the existence of sub-surface oxygen can be obtained by comparing the DFT-predicted surface elevation to experimental measurements. As shown in Fig. 3(c) and (d), sub-surface oxygen atoms cause the surface to rise by 1.7 Å. This height is comparable to the 1.8 Å elevation measured by STM [30].

While the energetic and structural results presented in this section demonstrate the likely presence of sub-surface oxygen during step (iii) of the four-step Cu(100) oxidation process, they do not lead to the surface restructuring that we hypothesize is needed before Cu_2O can form. As such, we next investigate the surface restructuring induced by the presence of an additional oxygen molecule.

3.2. Missing-row reconstructed Cu(100) surfaces relaxed with an oxygen molecule

Using STM, Lahtonen et al. found that defects in a Cu_2O island play a role in the growth of additional oxide [31]. To test if this defect effect is present in the earlier stages of oxidation, we first examined the stability and structure of missing-row reconstructed Cu(100) surfaces with or without a copper point defect with an oxygen molecule located at the initial positions shown in Fig. 1(a). No significant structural and/or energetic changes were found. Based on these results, we believe that while defects play a role after Cu_2O island nucleation, they do not play a significant role in the transition from the missing-row reconstruction to Cu_2O island nucleation.

We next examined the effect of on- and sub-surface oxygen atoms on the structure of the missing-row reconstructed Cu(100) surface when it is exposed to an additional oxygen molecule. In Table 2, the surface-oxide energies are reported for relaxed surfaces without an oxygen molecule ("No O_2") and with an oxygen molecule at different initial positions [see Fig. 1(a)]. In Fig. 4, we plot the E_S of each surface relaxed without an oxygen molecule and the minimum E_S of the surface relaxed with an oxygen molecule from Table 2 to highlight the effects of oxygen-induced surface restructuring.

When extra oxygen atoms are added to the on-surface sites and the surfaces are relaxed without an oxygen molecule, E_S drops for 2hol7 and 2hol78, while E_S for 2hol8 shows a much smaller decrease. This result indicates that the hol7 sites are more effective at stabilizing the surface than the hol8 sites. The hol7 site is surrounded by four copper atoms and is the most favorable adsorption site for atomic oxygen [13]. The hol8 site, however, has only two nearest-neighbor copper atoms because of the missing-row and is thus less effective at stabilizing the surface.

While E_S decreases in the presence of on-surface oxygen atoms, E_S for the majority of the surfaces relaxed with an extra oxygen molecule is comparable to or greater than that of the surfaces relaxed without an oxygen molecule. The exceptions are 2hol8 (FCC, BFC, and PMR) and 2hol78 (BFC and PMR). In the relaxed structures of 2hol8 FCC and BFC, we found that the oxygen molecule or dissociated oxygen atom adsorbs at the stabilizing hol7 site. In the relaxed structures of 2hol8 PMR, 2hol78 BFC, and 2hol78 PMR, there is further elevation of the top copper atoms. We attribute this elevation to repulsion between the oxygen molecule and the adsorbed oxygen atom at hol8 (2hol8 PMR and 2hol78 PMR) or hol7 (2hol78 BFC). This further surface elevation induces a decrease in E_S. In all cases, there is no significant surface restructuring (i.e., no formation of oxide-like structures). These findings indicate that extra oxygen atoms on the on-surface adsorption sites are not sufficient to induce the transition from the missing-row reconstruction to Cu_2O island formation. We therefore need to investigate the role of sub-surface oxygen.

For the missing-row reconstructed surfaces including sub-surface oxygen, the E_S of surfaces without an oxygen molecule decreases with increasing sub-surface oxygen coverage. The minimum E_S is predicted for the 2octa123 structure. For surfaces relaxed with an oxygen molecule, as shown in Table 2 and Fig. 4, a higher sub-surface oxygen coverage makes E_S decrease. The smallest E_S is predicted for 2octa1234 FCC. This structure also has the most severe surface restructuring [see Fig. 5(e) and (f)].[3] Comparing the surfaces relaxed with an oxygen molecule ("With O_2") to the surfaces relaxed without an oxygen molecule ("No O_2") in Fig. 4, we find that E_S decreases more and that there is more severe surface restructuring for 2octa12 FCC and

[2] We tested all distinct structures at 0.25 ML sub-surface oxygen coverage (2octa1, 2octa2 and 2octa4). The minimum E_S and the maximum elevation of the top copper atoms are found for 2octa2.

[3] To prevent unrealistically high forces caused by small interatomic distance in the unrelaxed structures, we added 20% to the gap between the top and second copper layer of 2octa1234 FCC and relaxed the structure. An identical surface restructuring was found.

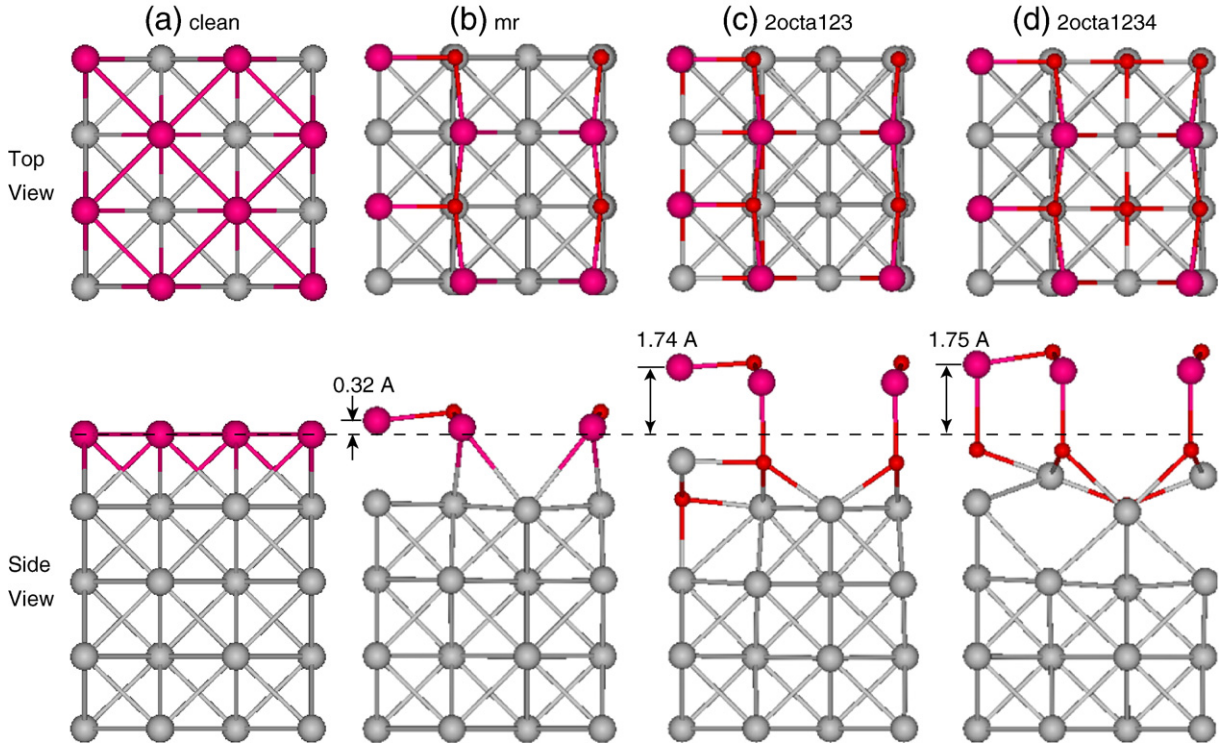

Fig. 3. Top and side views of (a) the clean Cu(100) surface, (b) the missing-row reconstruction (mr), and missing-row reconstructed surfaces relaxed with sub-surface oxygen atoms [(c) 2octa123 and (d) 2octa1234].

2octa1234 FCC compared to 2octa123 PMR [see Fig. 5(a)–(f)]. Severe surface restructuring thus leads to a more stable structure.

This surface restructuring, as shown in Fig. 5(a), (b), (e), and (f), leads to the formation of tetrahedral structures that are similar to the bulk Cu_2O structures shown in Fig. 5(g) and (h). Such tetrahedral structures are only found in 2octa12 FCC and 2octa1234 FCC. The tetrahedral structures found in 2octa1234 FCC have similar bond lengths and bond angles as found in bulk Cu_2O. To check for size effects, we also relaxed the 2octa12 and 2octa1234 structures in the $p\left(4\sqrt{2}\times 4\sqrt{2}\right)$ unit cell with and without an additional oxygen molecule. The tetrahedral structure was observed in both structures. Comparing the $p\left(2\sqrt{2}\times 2\sqrt{2}\right)$ and $p\left(4\sqrt{2}\times 4\sqrt{2}\right)$ unit cells in Table 2, the bigger unit cell has a higher E_S value because there are fewer tetrahedral structures per unit-area.

To further study the Cu_2O-like structures, we now investigate the net charges on the copper and oxygen ions predicted using the Bader

Table 2
Surface-oxide energy, E_S, of missing-row reconstructed Cu(100) surfaces including extra oxygen atoms at the on- and/or sub-surface sites [see Fig. 2(a) and (b)]. In the columns below E_S, the results for surfaces relaxed without or with an additional oxygen molecule are provided. For the surfaces relaxed with an additional oxygen molecule, we use four different initial positions: fcc hollow (FCC), between fcc hollow and Cu_S (BFC), perpendicular to missing-row (PMR), and parallel to missing-row (RMR) [see Fig. 1(a)]. The unit cell area is 53.290 Å^2 for $p\left(2\sqrt{2}\times 2\sqrt{2}\right)$ and 213.16 Å^2 for $p\left(4\sqrt{2}\times 4\sqrt{2}\right)$. E_S values in bold correspond to the oxide-like structures, some of which are shown in Fig. 5(a), (b), (e), and (f).

Index	On- [*ML*]	Sub- [ML]	Unit cell	E_S [eV/Å^2]				
				No O^2	FCC	BFC	PMR	RMR
mr	0.50	0.00	$p\left(2\sqrt{2}\times 2\sqrt{2}\right)$	0.045	0.054	0.044	0.046	0.060
2hol7	0.75	0.00	$p\left(2\sqrt{2}\times 2\sqrt{2}\right)$	0.006	0.020	0.013	0.006	0.020
2hol8	0.75	0.00	$p\left(2\sqrt{2}\times 2\sqrt{2}\right)$	0.039	0.026	0.018	0.032	0.053
2hol78	1.00	0.00	$p\left(2\sqrt{2}\times 2\sqrt{2}\right)$	0.003	0.015	−0.008	0.001	0.006
octa12	0.50	0.25	$p(2\sqrt{2}\times 2\sqrt{2})$	0.022	0.008	0.026	0.014	0.015
2octa2	0.50	0.25	$p\left(2\sqrt{2}\times 2\sqrt{2}\right)$	0.010	0.015	0.056	0.008	0.020
2octa12	0.50	0.50	$p\left(2\sqrt{2}\times 2\sqrt{2}\right)$	−0.016	**−0.025**	0.073	−0.024	0.000
2octa12	0.50	0.50	$p\left(4\sqrt{2}\times 4\sqrt{2}\right)$	−0.016	**−0.019**	0.004	−0.020	−0.013
2octa14	0.50	0.50	$p\left(2\sqrt{2}\times 2\sqrt{2}\right)$	−0.012	−0.010	−0.016	−0.015	−0.013
2octa23	0.50	0.50	$p\left(2\sqrt{2}\times 2\sqrt{2}\right)$	−0.030	−0.028	−0.028	−0.030	−0.014
octa1234	0.50	0.50	$p\left(2\sqrt{2}\times 2\sqrt{2}\right)$	−0.005	−0.018	−0.017	−0.022	−0.015
2octa123	0.50	0.75	$p\left(2\sqrt{2}\times 2\sqrt{2}\right)$	−0.057	−0.055	−0.056	−0.060	−0.042
2octa1234	0.50	1.00	$p\left(2\sqrt{2}\times 2\sqrt{2}\right)$	−0.051	**−0.102**	−0.066	−0.074	−0.034
2octa1234	0.50	1.00	$p\left(4\sqrt{2}\times 4\sqrt{2}\right)$	−0.051	**−0.079**	**−0.079**	−0.053	−0.047

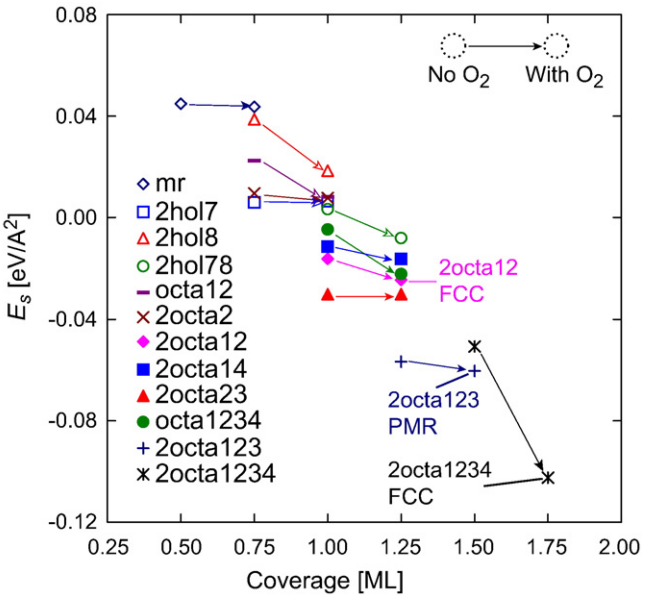

Fig. 4. Surface-oxide energy vs. oxygen coverage on the missing-row reconstructed Cu (100) surface with extra on- and sub-surface oxygen atoms. For each index, E_S is plotted for the case without an additional oxygen molecule and the minimum value found in the presence of an additional oxygen molecule (see data in Table 2). For each index, the E_S of the surface relaxed without an oxygen molecule ("No O_2") is connected to that of the surface relaxed with an oxygen molecule ("With O_2") by an arrow.

decomposition of charge density [49,50]. We first calculated the charges in bulk Cu_2O (−1.0 for oxygen and 0.5 for copper) and CuO (−1.0 for oxygen and 1.0 for copper). We then calculated the charge on all atoms in the missing-row reconstructed surface as the sub-surface oxygen coverage increases. The results are plotted in Fig. 6(a) and (b) vs. the position normal to the surface measured from the fixed bottom layer. As seen in Fig. 6(a), the oxygen atoms from the additional oxygen molecule have charges between −0.4 and −0.1. The charges on the atomic oxygens are around −1.0, which is the bulk Cu_2O value. The copper charges are shown in Fig. 6(b). In the bulk-like copper layers between 0 and 4 Å, the charge is around 0. In the missing-row reconstructed surface (mr), the copper charge is 0 for the bottom four layers because there is no sub-surface oxygen. In surfaces that contain sub-surface oxygen, the copper charge increases between 4 Å and 6 Å. Above 6 Å, the surface restructuring leads to copper charges between 0.5 and 1.0, a range between the bulk CuO and Cu_2O copper charges. This result further confirms the presence of oxide-like structures.

The projected density of state (PDOS) for the oxygen and copper atoms in the 2octa1234 tetrahedral structure [see Fig. 5(e) and (f)] and bulk Cu_2O [see Fig. 5(g) and (h)] are shown in Fig. 7(a) and (b). The oxygen *p*-band center and the copper *d*-band center are calculated using the first moment of the PDOS referenced to the Fermi level. The results are shown in Fig. 7(a) and (b) as vertical lines. The root mean square (rms) band width is calculated from the square root of the second moment of the PDOS [51].

As shown in Fig. 7(a), the PDOS of oxygen *p*-orbitals in 2octa1234 FCC and bulk Cu_2O have similar shapes. The rms band widths are 5.52 and 5.20 eV for 2octa1234 FCC and bulk Cu_2O. For the copper *d*-

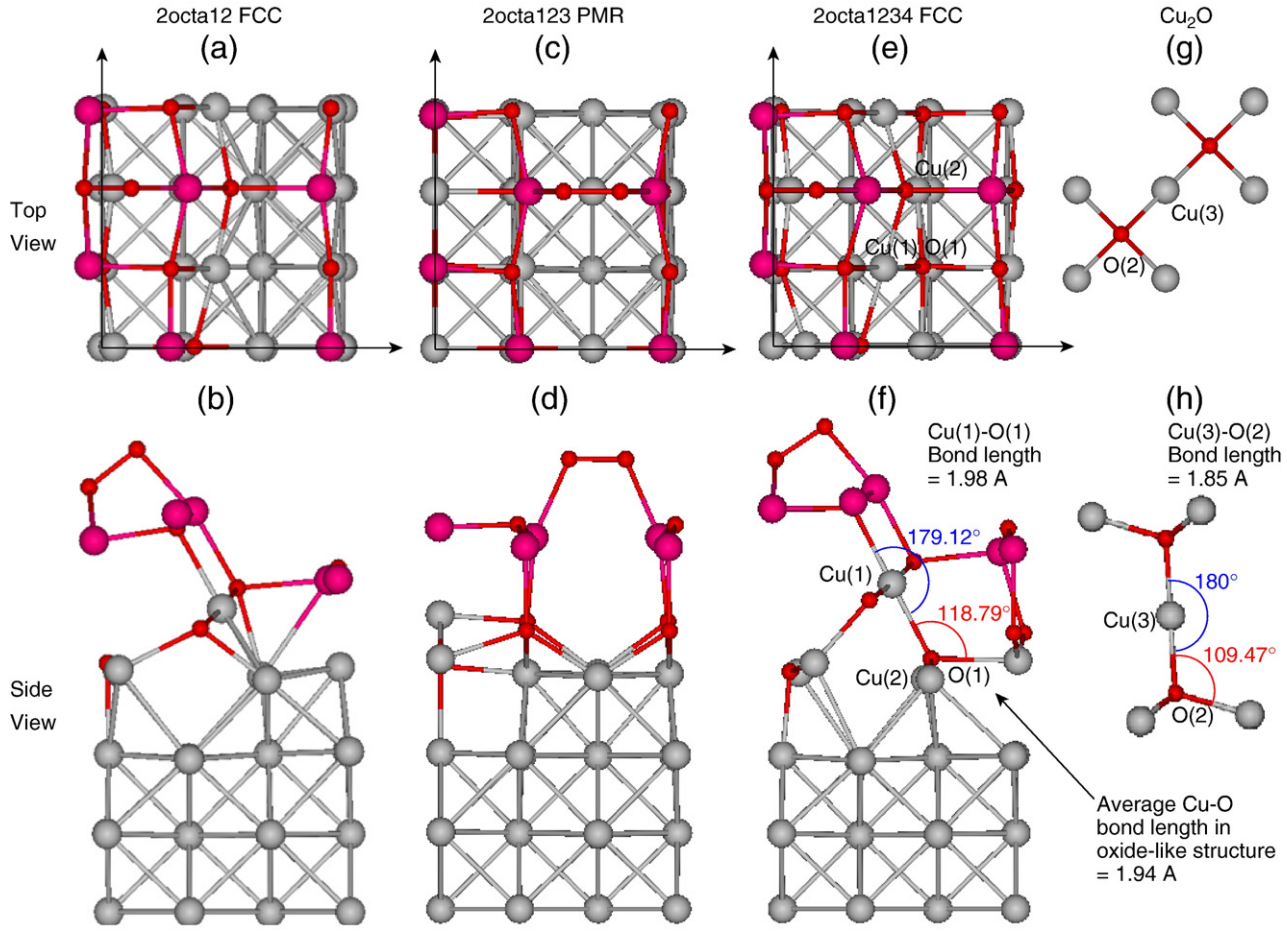

Fig. 5. Oxygen-molecule induced surface restructuring on the missing-row reconstructed Cu(100) surface with extra on- and sub-surface oxygen atoms: (a) top and (b) side views of 2octa12 FCC. (c) Top and (d) side views of 2octa123 PMR. (e) Top and (f) side views of 2octa1234 FCC. (g), (h) O–Cu–O bond in bulk Cu_2O.

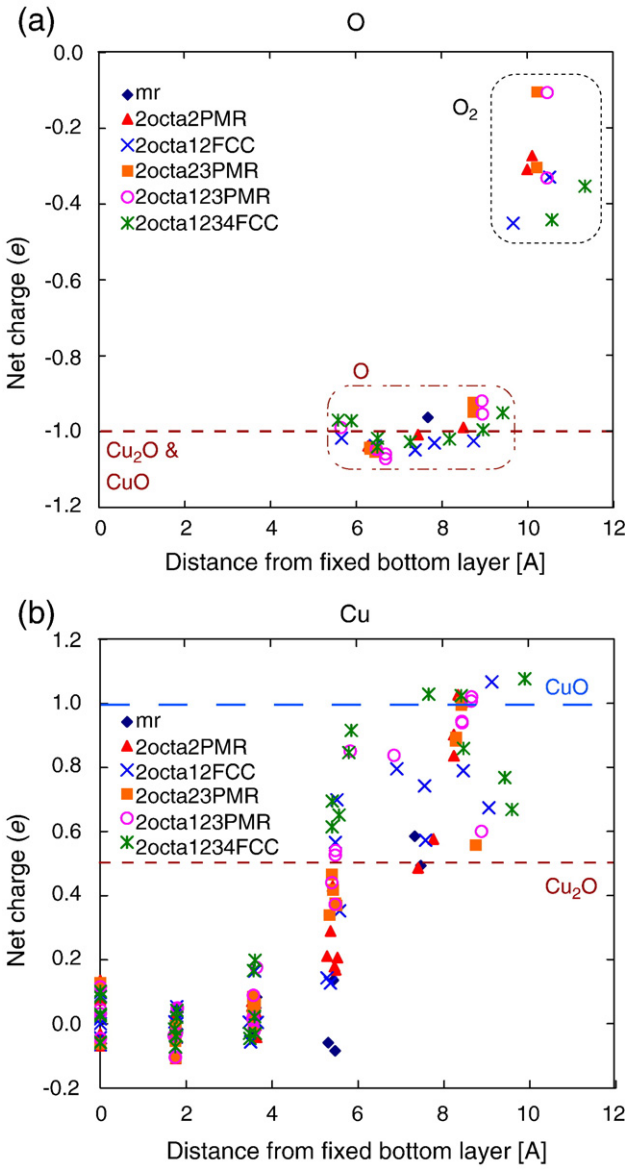

Fig. 6. Bader net charge vs. position measured from the fixed bottom layer for (a) oxygen and (b) copper atoms in surfaces relaxed with an oxygen molecule at different sub-surface oxygen coverages. The charges for atoms in bulk CuO and Cu_2O are provided as dashed lines.

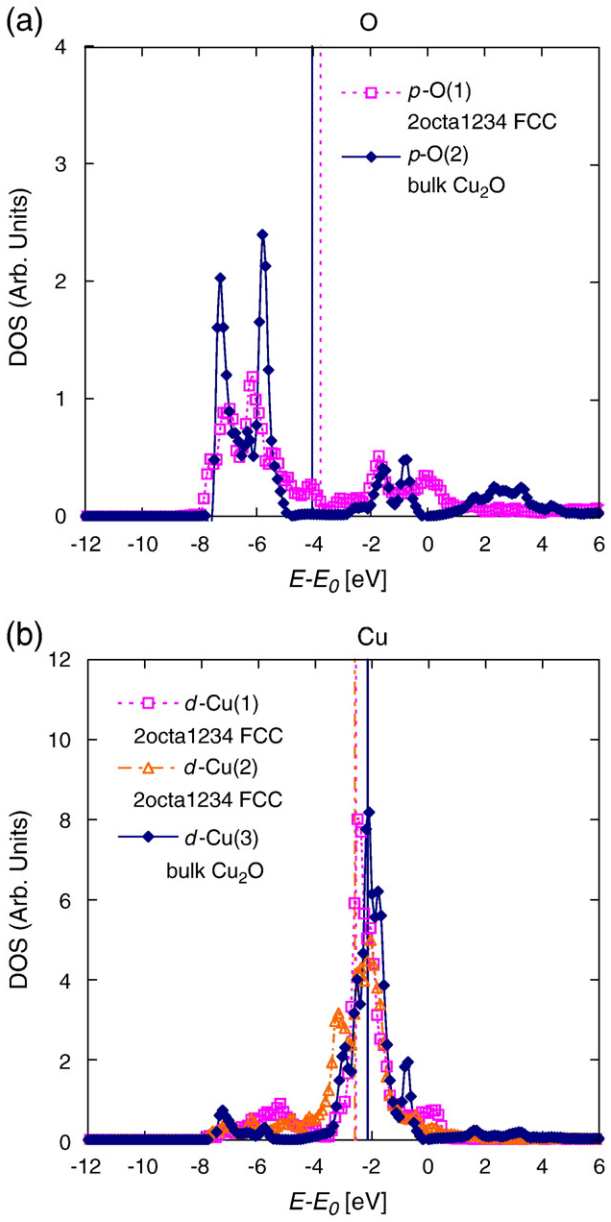

Fig. 7. Density of states for the (a) *p*-O and (b) *d*-Cu orbitals in the oxide-like 2octa1234 FCC and bulk Cu_2O. The atomic indices are shown in Figs. 5(c), (d), (e), and (f). The average energies of each *d*- and *p*-orbital (*d*-band center and *p*-band center) are shown with dashed and solid vertical lines for 2octa1234 FCC and bulk Cu_2O.

orbital, as shown in Fig. 7(b), the PDOS of the oxide-like structure (2octa1234 FCC) and bulk Cu_2O also have similar features. The rms band widths for Cu(1) and Cu(2) in 2octa1234 FCC are 3.35 and 3.42 eV, which is comparable to the value of 3.00 eV for bulk Cu_2O. During the transition from 2octa1234 FCC to bulk Cu_2O, the oxygen *p*-band center shifts downward by 0.29 eV and the copper *d*-band center shifts 0.42 eV upward for Cu(1) and 0.46 eV upward for Cu(2). This trend is opposite to the 0.4 eV downshift that a surface copper atom experiences during the earlier transition from the clean surface to the missing-row reconstruction [29].

4. Summary

Sub-surface oxygen plays a critical role in the formation of Cu_2O-like structures during the oxidation of a Cu(100) surface. In Section 3.1, we demonstrated the likely existence of sub-surface oxygen by comparing our DFT-predicted elevation of the top copper layer to previous STM measurements [see Fig. 3(c) and (d)]. When an oxygen molecule is added to the missing-row reconstructed Cu(100) surface, significant surface restructuring and oxide-like structures are observed when the sub-surface oxygen coverage increases. Such restructuring is not observed in the presence of copper point defects or extra oxygen atoms on the on-surface sites. We find similarity between these structures and bulk Cu_2O by analyzing their structure, net charges, and projected density of states [see Figs. 5(e), (f), 6(a), (b), and 7(a), (b)]. Based on the observed similarities, we believe that an increase in the sub-surface oxygen coverage is the key mechanism by which the missing-row reconstruction transitions to oxide formation.

Acknowledgements

This work is supported by the United States Department of Energy (Grant No. DOE FGOA01ER45919). We thank Professors John Kitchin, Simon Phillipot, and Susan Sinnott for providing computational resources. We thank Professor Judith Yang for helpful discussions.

Appendix A. Supplementary data

Supplementary data associated with this article can be found, in the online version, at doi:10.1016/j.susc.2010.05.004.

References

[1] G. Paul, R. Ghosh, S. Bera, S. Bandyopadhyay, T. Sakurai, K. Akimoto, Chem. Phys. Lett. 463 (2008) 117.
[2] B. Yuhas, P. Yang, J. Am. Chem. Soc. 131 (2009) 3756.
[3] G. Ostapenko, A. Cox, L. Ostapenko, J. Solid State Electrochem. 6 (2002) 245.
[4] T. Huang, D. Tsai, Catal. Lett. 87 (2003) 173.
[5] B. White, M. Yin, A. Hall, D. Le, S. Stolbov, T. Rahman, N. Turro, S. O'Brien, Nano Lett. 6 (2006) 2095.
[6] P.S. Bagus, F. Illas, Phys. Rev. B 42 (1990) 10852.
[7] T. Lederer, D. Arvanitis, G. Comelli, L. Troger, K. Baberschke, Phys. Rev. B 48 (1993) 15390.
[8] T. Wiell, J.E. Klepeis, P. Bennich, O. Bjorneholm, N. Wassdahl, A. Nilsson, Phys. Rev. B 58 (1998) 1655.
[9] S. Liem, J. Clarke, G. Kresse, Surf. Sci. 459 (2000) 104.
[10] Y. Xu, M. Mavrikakis, Surf. Sci. 494 (2001) 131.
[11] L. Padilla-Campos, P. Fuentealba, Theor. Chem. Acc. 110 (2003) 414.
[12] Z.X. Wang, F.H. Tian, J. Phys. Chem. B 107 (2003) 6153.
[13] M. Alatalo, S. Jaatinen, P. Salo, K. Laasonen, Phys. Rev. B 70 (2004) 245417.
[14] A. Puisto, H. Pitkanen, M. Alatalo, S. Jaatinen, P. Salo, A.S. Foster, T. Kangas, K. Laasonen, Catal. Today 100 (2005) 403.
[15] M. Alatalo, A. Puisto, H. Pitkanen, A. Foster, K. Laasonen, Surf. Sci. 600 (2006) 1574.
[16] T. Fujita, Y. Okawa, Y. Matsumoto, K. Tanaka, Phys. Rev. B 54 (1996) 2167.
[17] S. Stolbov, A. Kara, T.S. Rahman, Phys. Rev. B 66 (2002) 245405.
[18] H.C. Zeng, R.A. McFarlane, K.A.R. Mitchell, Surf. Sci. 208 (1989) L7.
[19] F. Jensen, F. Besenbacher, E. Laegsgaard, I. Stensgaard, Phys. Rev. B 42 (1990) 9206.
[20] K.W. Jacobsen, J.K. Norskov, Phys. Rev. Lett. 65 (1990) 1788.
[21] F.M. Leibsle, Surf. Sci. 337 (1995) 51.
[22] D. Sekiba, T. Inokuchi, Y. Wakimoto, K. Yagi-Watanabe, H. Fukutani, Surf. Sci. 470 (2000) 43.
[23] M. Kittel, M. Polcik, R. Terborg, J.-T. Hoeft, P. Baumgartel, A. Bradshaw, R. Toomes, J.-H. Kang, D. Woodru€, M. Pascal, C. Lamont, E. Rotenberg, Surf. Sci. 470 (2001) 311.
[24] S. Stolbov, T.S. Rahman, Phys. Rev. Lett. 89 (2002) 116101.
[25] M.J. Harrison, D.P. Woodruff, J. Robinson, W.P.D. Sander, J. Kirschner, Phys. Rev. B 74 (2006) 165402.
[26] N. Bonini, A. Kokalj, A.D. Corso, S. de Gironcoli, S. Baroni, Surf. Sci. 600 (2006) 5074.
[27] H. Iddir, D.D. Fong, P. Zapol, P.H. Fuoss, L.A. Curtiss, G.-W. Zhou, J.A. Eastman, Phys. Rev. B 76 (2007) 241404 (R).
[28] X. Duan, O. Warschkow, A. Soon, B. Delley, C. Stampfl, Phys. Rev. B 81 (2010) 075430.
[29] S. Jaatinen, J. Blomqvist, P. Salo, A. Puisto, M. Alatalo, M. Hirsimaki, M. Ahonen, M. Valden, Phys. Rev. B 74 (2007) 075402.
[30] M. Lampimaki, K. Lahtonen, M. Hirsimaki, M. Valden, J. Chem. Phys. 126 (2007) 034703.
[31] K. Lahtonen, M. Hirsimaki, M. Lampimaki, M. Valden, J. Chem. Phys. 129 (2008) 124703.
[32] J.C. Yang, B. Kolasa, J.M. Gibson, M. Yeadon, Appl. Phys. Lett. 73 (1998) 2841.
[33] G. Zhou, J.C. Yang, Phys. Rev. Lett. 89 (2002) 106101.
[34] G. Zhou, J.C. Yang, Appl. Surf. Sci. 210 (2003) 165.
[35] G. Zhou, J.C. Yang, Surf. Sci. 559 (2004) 100.
[36] G. Zhou, J.C. Yang, J. Mater. Res. 20 (2005) 1684.
[37] N. Cabrera, N.F. Mott, Rep. Prog. Phys. 12 (1948) 163.
[38] T. Kangas, K. Laasonen, A. Puisto, H. Pitkanen, M. Alatalo, Surf. Sci. 584 (2005) 62.
[39] T. Kangas, K. Laasonen, Surf. Sci. 602 (2008) 3239.
[40] M. Lee, A.J.H. McGaughey, Surf. Sci. 603 (2009) 3404.
[41] G. Kresse, J. Hafner, Phys. Rev. B 47 (1993) 558.
[42] G. Kresse, J. Hafner, Phys. Rev. B 49 (1994) 14251.
[43] G. Kresse, J. Hafner, J. Phys.: Condens. Matter 6 (1994) 8245.
[44] G. Kresse, J. Furthmuller, Comput. Mat. Sci. 6 (1996) 15.
[45] G. Kresse, J. Furthmuller, Phys. Rev. B 54 (1996) 11169.
[46] J.P. Perdew, J.A. Chevary, S.H. Vosko, K.A. Jackson, M.R. Pederson, D.J. Singh, C. Fiolhais, Phys. Rev. B 46 (1992) 6671.
[47] H.J. Monkhorst, J.D. Pack, Phys. Rev. B 13 (1976) 5188.
[48] I. Batyrev, A. Alavi, M.W. Finnis, Faraday Discuss. 144 (1999) 33.
[49] R.F.W. Bader, Atoms in Molecules: A Quantum Theory, Oxford University Press, Oxford, 1990.
[50] G. Henkelman, A. Arnaldsson, H. Jonsson, Comput. Mat. Sci. 36 (2006) 354.
[51] J. Kitchin, J. Norskov, M. Barteau, J. Chen, J. Chem. Phys. 120 (2004) 10240.